

**OXYGEN ISOTOPIC COMPOSITIONS OF HYDRATED INTERPLANETARY DUST PARTICLES: IMPLICATIONS FOR AQUEOUS ALTERATION IN OUTER SOLAR SYSTEM OBJECTS.** L. P. Keller<sup>1</sup>, and C. J. Snead<sup>2,3</sup>. <sup>1</sup>ARES, Code XI3, NASA-JSC, 2101 NASA Parkway, Houston, TX 77058, USA (Lindsay.P.Keller@nasa.gov), <sup>2</sup>JETS, NASA Johnson Space Center, Houston TX 77058, USA. <sup>3</sup>Texas State University, San Marcos, 601 University Dr, San Marcos, TX 78666, USA.

**Introduction:** The oxygen isotopic compositions of meteoritic materials are widely believed to reflect mixing between <sup>16</sup>O-rich and <sup>16</sup>O-poor reservoirs that formed via CO self-shielding in the protoplanetary disk [1] or in the protosolar molecular cloud [2]. The self-shielding model predicts the formation of <sup>17,18</sup>O-rich water that subsequently reacted with primitive nebular and presolar dust in the protoplanetary disk. We are searching for evidence of this heavy water reservoir through coordinated mineralogical and isotopic analyses of hydrated carbon-rich interplanetary dust particles (IDPs). A subset of these hydrated IDPs contain high solar flare track densities consistent with an origin in outer Solar System bodies such as Edgeworth-Kuiper belt objects (EKBOs) [3]. EKBOs formed at large heliocentric distances beyond the gas giant planets and are believed to have avoided much of the high temperature processing experienced by asteroidal bodies in the inner solar system. Here, we report on our coordinated high-precision oxygen isotopic measurements and transmission electron microscope analyses and implications for aqueous alteration in outer solar system bodies.

**Materials and Methods.** We analyzed 6 IDPs: U2153L1, U2153M1, L2083D58, L2076C10, L2071E39, and L2098B1. The U2153L1 and M1 are related fragments from the same cluster (U2153#4). The IDPs were embedded in elemental sulfur and partly sectioned using ultramicrotomy to produce thin sections ~50 nm thick for transmission electron microscopy measurements as well as NanoSIMS measurements of H, N, and O isotopes. Fourier-transform infrared (FTIR) spectra were obtained either from microtome thin sections, or in reflectance mode from particles pressed into Au. The unmicrotomed portion of each IDP was removed from the sulfur and was fixed to 1" diameter, 1/8" thick polished aluminum disks for quantitative electron microprobe elemental analysis (including C) and secondary ion mass spectrometry (SIMS) oxygen isotope analysis using three different mounting methods. Harder IDPs were pressed into 0.01" thick, 99.999% (five nines) pure gold foil that had been annealed at 800°C and cleaned with HF. Based on experiments with Orgueil matrix, we found that more friable hydrated materials would not embed into the annealed gold; softer IDPs were instead pressed into pure (six nines) indium metal. While In metal exhibited a higher oxygen background than the HF-cleaned gold, the

small raster size of the Cs primary beam we utilized ensured O-isotope measurements excluded any In background signal. For the IDP embedded in epoxy, we trimmed away the surrounding epoxy, removed the small (~50µm) cube containing the sample and pressed the cube into indium.

Quantitative chemical compositions were obtained using a Cameca SX-100 electron microprobe (EPMA) operated at 10 kV to measure multiple spots on the pressed IDPs prior to the ion probe analyses.

The IDPs were analyzed for 3-oxygen isotopic compositions at UCLA with the Cameca IMS-1290 ion microprobe using a 10KV, 70 pA Cs+ primary beam and a 10 µm raster; normal incidence electron flooding was used for charge compensation. Secondary ions were measured via multicollection, with <sup>16</sup>O ions counted on a faraday cup and <sup>17</sup>O and <sup>18</sup>O ions counted on electron multipliers. A mass resolving power of 7000 was used to separate the interfering <sup>16</sup>OH<sup>-</sup> peak from the <sup>17</sup>O<sup>-</sup> signal. San Carlos olivine, Burma spinel and Afrique magnetite were used as standards to correct for instrumental mass fractionation.

**Mineralogy.** TEM analyses of the IDPs were interrupted by the Covid shutdown, but in general the hydrated IDPs in this study are compact low-porosity objects with a mineralogy dominated by fine-grained saponite and lesser serpentine that are Mg-rich except in C10 and E39 which appear to have been strongly heated. The phyllosilicates are intimately associated with finely dispersed Fe,Ni-sulfide grains (pyrrhotite and pentlandite) and minor bruenneritic (Mg-Fe) carbonates or their thermal decomposition products. Rare grains of anhydrous silicates such as forsterite, enstatite, diopside, and quartz are observed and commonly contain solar flare tracks. The preservation of solar flare tracks and minerals with low decomposition temperatures suggest that these IDPs were not strongly heated during atmospheric entry, consistent with low atmospheric entry velocities [4].

**Organic Matter.** We measured the bulk composition of the remainder of the IDPs that were pressed into Au or In prior by EPMA. The chemical compositions are generally within a factor of 2 of CI abundances except for C, which is typically highly enriched over CI values. Individuals and clusters of carbon nanoglobules occur in several of the IDPs in addition to abundant carbonaceous material finely dispersed

throughout matrix. We obtained detailed TEM energy-dispersive X-ray (EDX) and electron energy-loss spectroscopy (EELS) analyses of globules in U2153M1 [5] and found that they are chemically zoned with rims that enriched in O and depleted in S. EELS mapping of globules reveals higher C=O functionality in globule rims compared to their cores that is believed to result from aqueous alteration [5]. Infrared spectra from M1, L1, and D58 show strong aliphatic C-H stretches consistent with the presence of short-chain aliphatic hydrocarbons in these IDPs.

**Isotopic Compositions.** The oxygen isotopic compositions measured in the 6 IDPs are plotted on 3 isotope diagram Figure 1 and all plot within error of the CCAM line. For several of the IDPs we were able to obtain multiple analyses (Table 1). The  $\Delta^{17}\text{O}$  values range from -23‰ in U2153M1 up to +3.4‰ in U2153L1. The 10 $\mu\text{m}$  raster used for these analyses was sufficiently compact to analyze multiple areas of individual IDPs – especially larger IDPs that were flattened and spread out on the Au substrate.

**Results and Discussion.** The O isotopic data from the 6 hydrated IDPs in this study all fall on a slope 1 line. U2153M1 contains a nearly pure forsterite grain several  $\mu\text{m}$  in size that is the likely host for the  $^{16}\text{O}$ -rich measurement. The O isotopic compositions of B1, L1, D58 plot above the TFL and are distinct from known hydrated carbonaceous chondrite meteorites. The overall slope 1 trend also differs from known carbonaceous chondrite groups which show shallower slopes because of mass dependent fractionation of O isotopes during alteration (e.g. slope 0.5 for CI [1], slope  $\sim 0.7$  for CR [6]). We previously suggested that amorphous silicate grains with nanophase inclusions of FeNi metal and sulfides were the precursors to the phyllosilicates in hydrated IDPs [4]. The FeS-free average composition of amorphous silicates in anhydrous IDPs is highly enstatite normative with an average Mg/Si atomic ratio nearly the same as in saponite [7]. We hypothesize that the main alteration reactions involved: 1) the oxidation of Fe metal in the amorphous silicate precursors to  $\text{Fe}^{2+}$  and  $\text{Fe}^{3+}$ , similar to the manner in which cosmic symplectite formed [8, 9], and 2) the incorporation of  $\text{H}_2\text{O}$  into the anhydrous amorphous silicates to form phyllosilicates, thus keeping the O isotopic compositions on a slope 1 line.

**Acknowledgements:** This study was supported by NASA ISFM funding to LPK. We thank Ming-Chang Liu and Kevin McKeegan for assistance and access to the UCLA Cameca ims-1290.

**References:** [1] Clayton, R. N. (2002) *Nature*, 415, 860. [2] Yurimoto, H. & Kuramoto, K. (2004) *Science*, 305, 1763. [3] Keller, L. P. and Flynn, G. J. (2019)

*LPSC 50<sup>th</sup>*, #2525. [4] Keller, L. P. & Snead, C. J. (2020) *LPSC 51<sup>st</sup>*, #2314. [5] Keller, L. P. *et al.* (2019) *MAPS*, #6438. [6] Schrader, D. J. *et al.* (2011) *GCA* 75, 308. [7] Keller, L. P. & Messenger, S. (2011) *GCA* 75, 5336. [8] Sakamoto, N. *et al.* (2007) *Science*, 317, 231. [9] Nguyen, A. N. *et al.* (2017) *MAPS* 52, 2004.

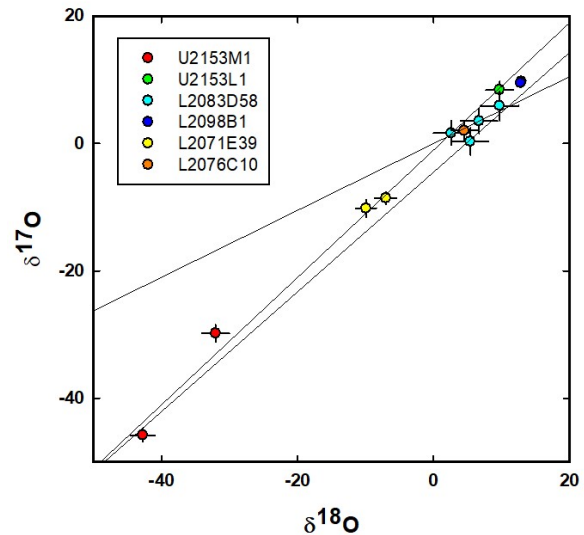


Figure 1. Three isotope plot showing the compositions of the hydrated IDPs in this study (TFL: terrestrial fraction line, YR: Young-Russell line, CCAM: carbonaceous chondrite anhydrous minerals mixing line).

IDP	$\delta^{18}\text{O}$	$2\sigma$	$\delta^{17}\text{O}$	$2\sigma$	$\Delta^{17}\text{O}$	$2\sigma$
U2153M1_1	-42.7	1.8	-45.8	1.0	-23.6	1.4
U2153M1_2	-32.0	2.0	-29.8	1.3	-13.2	1.5
U2153L1-1	9.7	2.0	8.4	1.3	3.4	1.5
L2076C10	4.5	1.9	2.0	1.4	-0.3	1.5
L2071E39_1	-7.0	1.6	-8.6	0.9	-5.0	1.3
L2071E39_2	-9.9	1.5	-10.2	1.4	-5.1	1.5
L2083D58_1	9.7	2.8	5.9	2.3	0.9	1.9
L2083D58_2	2.6	2.6	1.6	1.9	0.2	1.8
L2083D58_3	5.4	2.7	0.3	2.1	-2.5	1.9
L2083D58_4	6.7	2.7	3.5	2.0	0.0	1.8
L2098B1_1	12.9	0.5	9.7	0.7	3.0	1.0
L2098B1_2	12.8	0.5	9.5	0.7	2.8	1.0

Table 1. Oxygen isotopic data and  $2\sigma$  errors for the hydrated IDP data in Figure 1.